

Differential-Phase Reflectometry and Electron Bernstein Wave Radiometry using Phased-array Antenna System in the QUEST

H. Idei¹⁾, K. Nagata²⁾, M. Sakaguchi²⁾, K. Dono²⁾, Y. Wataya²⁾, S. Ohdachi³⁾, S. Inagaki¹⁾, Y. Nagayama³⁾, K. Kawahata³⁾, H. Igami³⁾, T. Shimosuma³⁾, H. Zushi¹⁾, K. Hanada¹⁾, K. Nakamura¹⁾, M. Sakamoto¹⁾, M. Hassegawa¹⁾, Y. Higashizono¹⁾, S. Kawasaki¹⁾, H. Nakashima¹⁾, A. Higashijima¹⁾, Y. Takase⁴⁾, T. Maekawa⁵⁾, O. Mitarai⁶⁾ and Y. Kishimoto⁵⁾

¹⁾ *Research Institute for Applied Mechanics, Kyushu Univ., Kasuga, 816-8580, Japan*

²⁾ *Interdisciplinary Graduate School of Eng. Sci., Kyushu Univ., Kasuga, 816-8580, Japan*

³⁾ *National Institute for Fusion Science, Toki, 509-5292, Japan*

⁴⁾ *Department of Complexity Sci. and Eng., Univ. of Tokyo, Kashiwa 277-8561, Japan*

⁵⁾ *Graduate School of Energy Science, Kyoto Univ., Kyoto 606-8501, Japan*

⁶⁾ *Inst. of Industrial Sci. and Tech. Research, Tokai Univ., Kumamoto 862-8652, Japan*

(Received: 20 November 2009 / Accepted: 6 April 2010)

The differential-phase reflectometry has been developed to measure the density profile evolution, concerning electron Bernstein Wave (EBW) heating and current drive in the QUEST. The proper phase dependence was confirmed in developed single-side-band heterodyne differential-phase reflectometry at RIAM microwave/mm-wave test facilities. The phase time evolutions in the QUEST were also successfully measured, but the weak reflected-wave caused the small ratio of signal to noise in the measurements. The Phased Array Antenna (PAA) system was proposed for the reflectometry to obtain the large reflected-wave. The oblique viewing EBW emission can be measured by the precise phase-array measurements between the PAA waveguide elements. The PAA was confirmed to be effective, as a launching antenna for the reflectometry, and as a receiving antenna for the EBW radiometry.

Keywords: AM reflectometry, Electron Bernstein wave, phased-array antenna, QUEST

1. Introduction

Microwave reflectometry has been widely used to measure density profile and fluctuation in the fusion-research plasma. This technique is based on a phase delay measurement of a probing-wave propagating and reflected by a cutoff layer in the plasma. In general, since the wavelength of the probing-wave is much smaller to the propagating length, sometimes the phase jump was occurred in the homodyne detection. It induces to mistake the counting-up, which causes a phase runaway phenomenon what one call. The amplitude modulation (AM) reflectometry has been developed to measure correctly the phase delay in the probing-wave propagation. The AM of the probing-wave can be recognized as a beat between two frequencies. The AM reflectometry was sometimes called as a differential-phase reflectometry. The phase difference of two probing-wave frequencies was measured in the diode detection. Since the wavelength of the AM (differential) frequency was comparable to the propagating length, and the so-called runaway phenomenon never happen in the AM reflectometry.

Detailed density profile measurements are essential to study mode conversion phenomena in the spherical tokamak (ST) experiments. Electron Bernstein

Wave Heating and Current Drive (EBWH /CD) is one of attractive candidates of heating and current drive method to sustain the steady-state over-dense plasma in the ST. In the EBWH/CD, some mode conversions from an Electron Cyclotron electromagnetic Wave (ECW) to an Electron Bernstein electrostatic Wave (EBW) are required. In the Q-shu University Experiment with Steady State Spherical Tokamak (QUEST), the EBWH/CD experiments are planned at 8.2GHz, to sustain the steady-state ST plasma [1]. The density gradient where the ECW converts to the EBW is a key parameter to attain high conversion efficiency.

In the Compact PWI (Plasma-Wall Interaction) Device, that is the small ST device in Kyushu University, an AM reflectometer system was developed to measure the density profile with high time resolution (by the 10 μ s frequency switching) [2]. The developed system successfully measured the phase delay of the broadband (6-18GHz) reflected-wave at both the CPD vessel wall and the R-cutoff layers in the plasma. The performance of the CPD AM reflectometry was checked at RIAM microwave/mm-wave test facilities in detail. The reflected-wave intensity was same level to the direct coupling component between the launching and receiving antennae in the large propagat-

author's e-mail: idei@tri.riam.kyushu-u.ac.jp

ing length. The Single-Side-Band (SSB) heterodyne differential-phase reflectometry has been developed to treat separately the direct coupling component and the reflected-wave. The developed system was installed to measure the density profile in the QUEST, concerning the mode conversion study.

An EBW radiometry has been developed to measure time evolutions of electron temperature profiles in over-dense plasmas [3,4]. The Electron Cyclotron Emission (ECE) radiometry is widely used to measure the electron temperature time evolutions, but the ECE cannot propagate outside the plasma due to the cut-off in the over-dense plasma. The ECW converted from the EBW as a reversal process of the mode conversion for the EBWH/CD might propagate outside, and detected in the radiometry. The EBW radiometry is not only a powerful tool to measure the electron temperature time evolutions, but also to investigate the mode conversion phenomena. The mode conversion strongly depended on the density profile, the propagating polarization and the refractive index, $N_{//}$, in parallel to the magnetic field. The receiving angle and polarization in the EBW radiometry are important to clarify the mode conversion mechanism, together with the density profile measured with the reflectometry.

The Phased Array Antenna (PAA) was considered as a launching antenna of the probing-wave in the reflectometry, and as a receiving antenna in the EBW radiometry. The reflected-wave in the reflectometry was expected to be much stronger than the direct coupling component using the PAA. In the EBW radiometry, the receiving angle and polarization were measured with precise phase detection between the antenna elements. The prototype waveguide PAA was designed and fabricated. The antenna performance was checked in the low power test facilities.

This paper is organized as follows. Section 2 describes the SSB heterodyne differential-phase reflectometry. In Sections 3 and 4, the developed prototype PAA system for the reflectometry and the EBW radiometry are shown, and the conclusion is finally given in Section 5.

2. SSB Heterodyne Differential-Phase Reflectometry

2.1 Direct coupling effect

Figure 1 shows the phase evolution along the propagating length measured with the CPD AM reflectometry at the low power test facilities. In the test, the reflecting aluminum plate was moved to scan the propagating length. Here, x was the distance between the reflectometry antennae and the plate. The phase evolution along the propagation was expressed with a linear dependence $[2k_{AM}x]$ on the wave number

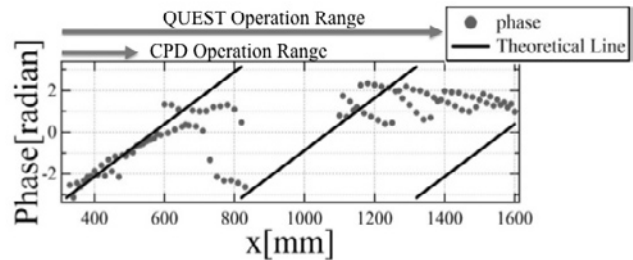


Fig. 1 : Phase evolution along the propagating length measured by the AM reflectometry developed for the CPD experiments.

k_{AM} of the AM frequency in the CPD operation range. In the large length range for the QUEST, the reflectometer could not detect the proper phase evolution. In the large propagating length, the detected phase was rapidly changed in the specific range with a period on the wavelength of the probing-wave along the propagation. In the figure, the aliasing evolution was appeared in the large-length operation range. There was interference in the reflected probing-wave and the other components of the probing-wave frequency. The direct coupling wave between launching and receiving antennae was considered as a counterpart for the interference. The differential-phase $[2(k_1 - k_2)x]$, or $[2k_{AM}x]$, in two frequencies $[\omega_1$ and $\omega_2]$ probing-wave should be measured at the diode detection in the AM reflectometry. The phases of the direct coupling components were expressed in terms of $[k_1x'$ and $k_2x']$ with a representative length x' for the coupling. Spurious phase differences $[2(k_1x - k_2x')$ and $2(k_1x' - k_2x)]$ were detected as cross terms at the interference in the diode detection. If the reflected signal level was much higher than the direct coupling level in the CPD operation range, the spurious components did not affect the detected phase well.

In the CPD AM reflectometry, the two frequency probing-waves were prepared in upper/lower-side bands (USB/LSB) at the up/down frequency converter [1]. In order to avoid the interference with the direct coupling wave, the USB and LSB components were separately measured in a heterodyne detection using an image rejection mixer. The intermediate frequency (IF) signal at the mixer was demodulated in an IQ operation, and the IF phase was measured at the IQ demodulation mixer. The differential-phase dependence $[2(k_1 - k_2)x]$ can be evaluated from subtraction of the LSB phase dependence from the USB phase dependence. This operation to detect the differential-phase was based on the SSB heterodyne detection technique. Figures 2 show Lissajous curves of the USB and LSB signals in the large propagation length range shown in Fig.1. The Lissajous curves were off-center. The offset coordinates expressed the direct coupling

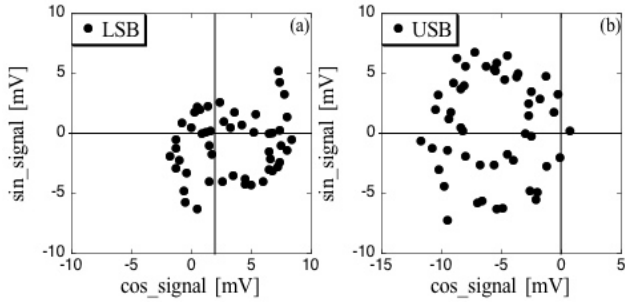


Fig. 2 : Lissajous curves of the (a): LSB and (b): USB phases in the SSB heterodyne differential-phase reflectometry.

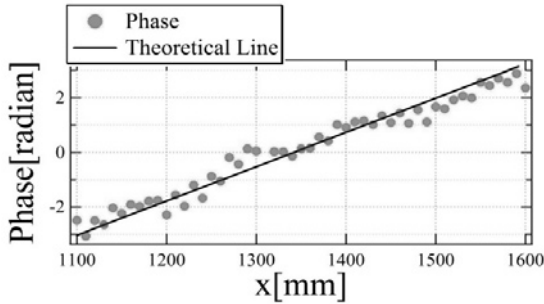


Fig. 3 : Phase evolution along the propagation in the developed SSB heterodyne differential-phase reflectometry.

IQ components. The offset was comparable to the Lissajous radius which showed the reflected signal amplitude. The radius or reflected signal amplitude was decreased along the propagation length, showing the spiral curve in the figure. In the larger propagation length, the center-offset (direct coupling) affected significantly the phase measurements in the diode detection at the AM reflectometry, and the measured phase were changed in the specific region of the Lissajous figure. Figure 3 shows the subtracted phase evolution along the propagation after the removal of the center-offset in the Lissajous figure. The measured phase evolution along the propagation was properly expressed with the linear dependence $[2k_{AM}x]$ on the wave number k_{AM} even in the large propagation length.

2.2 Phase time evolution measured in the QUEST

The developed SSB heterodyne differential phase reflectometer was installed to the QUEST. Figures 4 show time evolutions of the incident 8.2GHz RF power, the H_{α} intensity, the phases of the LSB/USB IF phases, and the subtracted phase in the developed reflectometer. The operating frequency was 8GHz, and the magnetic field was 0.137T. First the probing-wave was reflected at the inner wall of the QUEST vessel, and was reflected at the R-cutoff layer of the

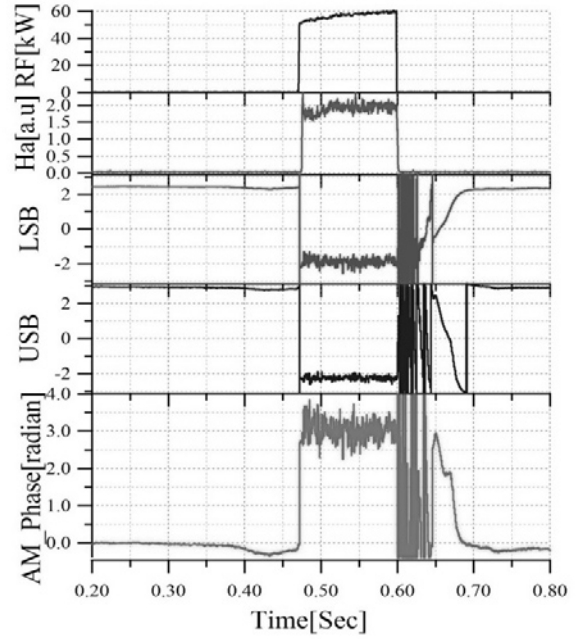


Fig. 4 : Time evolutions of the incident RF power, the H_{α} intensity, the measured phase of the LSB/USB IF phases, the subtracted phase in the SSB heterodyne differential-phase reflectometer.

major radius $R=0.7\text{m}$ when the plasma was produced by the incident 8.2GHz RF power of 50kW. The electron density at the R-cutoff layer of the 8GHz frequency was evaluated as $4.1 \times 10^{17} \text{ m}^{-3}$.

Figure 5 shows the Lissajous figure of the USB phase in the QUEST. The ratio of the reflected wave (or the Lissajous radius) to the direct coupling component (or the Lissajous offset) became small in the QUEST, compared to that in the low power test as shown in Figs.2. In the QUEST, the launching and receiving quad-ridged waveguide antennae were set in front of a quartz vacuum window. The inner wall of the QUEST vessel is not a plane. The reflected wave became weak in the QUEST setup. The subtracted phase in the developed SSB heterodyne differential-phase reflectometer did not show the proper density decay after turning off the RF injection due to the small reflected-wave signal, as shown in Figs.4. Figure 6 shows the counted fringe time evolutions of the LSB/USB phases and of the subtracted AM phase in the density decay. The propagating distances of the 8 GHz wave were about 2.6m and 1.6m at the wall- and the cutoff- reflections, respectively. The around 27 fringes should be counted in the density decay, but a number of the fringes (more than 100 fringes) were counted, as shown in Fig.6. The phase jump between the phases of $\pm\pi$ due to the small reflected-wave signal caused the fringe miscount in the density delay. The reflected-wave signal level should be essentially

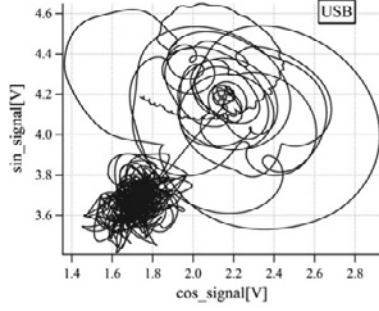


Fig. 5 : Lissajous figure of the USB phase in the QUEST.

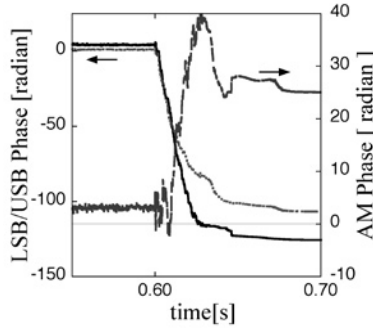


Fig. 6 : Counted fringe time evolutions of the LSB/USB phases and the subtracted AM phase in the density decay after turning of RF injection.

increased to measure the proper phase evolution. The PAA system was considered as a launching antenna in the reflectometry to receive the significant reflected-wave.

3. Prototype Phased-Array Antenna System

3.1 Reflectometry Use

The far field radiation is important for the reflectometry use in the larger propagating length. In the low operating frequency around 8GHz, the directionality of the quad-ridged antenna was not so good, and the diffraction effect was rather large. The direct coupling effect significantly affected the performance of the AM reflectometry in the low operating frequency.

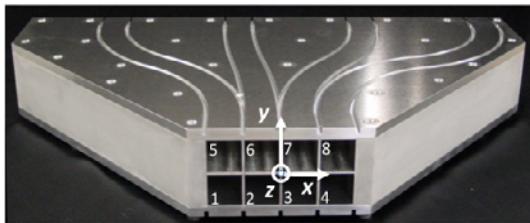


Fig. 7 : Developed prototype phased-array antenna. The coordinates in the low power test and the numbers of waveguide elements are also shown.

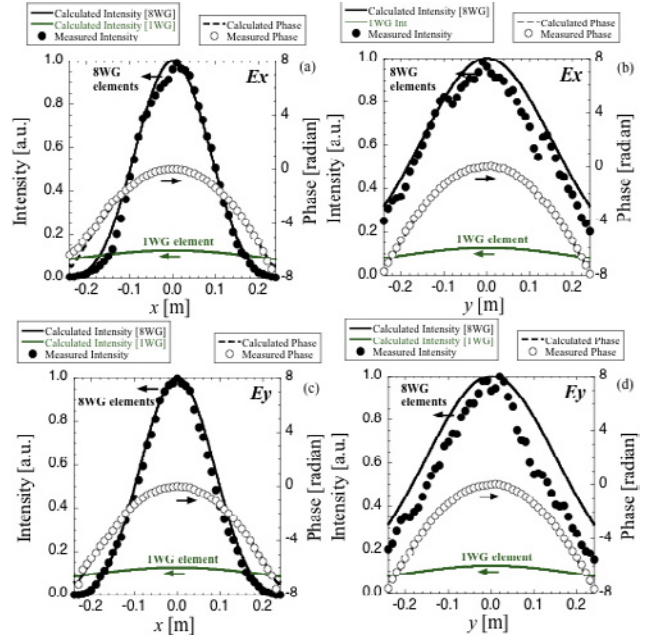


Fig. 8 : Measured field intensity and phase profile, and the calculated intensity and phase profiles with 1 waveguide element and 8 elements of the PAA at a radiation position of $z=600\text{mm}$. (a): $E_x(x)$, (b): $E_x(y)$, (c) $E_y(x)$ and (d) $E_y(y)$

It was expected the PAA system might focus the radiated field with good directionality even at the larger propagating length.

Figure 7 shows the developed prototype PAA with 8 [4 × 2] square waveguide elements. There were 8 square waveguide elements to excite two orthogonal electric field components. The phases between waveguide elements were adjusted to obtain a well-defined straight beam for the reflectometry. Figure 8 shows the field intensity and phase profiles, measured at the low power test facilities, at a radiated position of $z=600\text{ mm}$. Here, the phased-array was set as $[\Delta\phi_{2-1}, \Delta\phi_{3-1}, \Delta\phi_{4-1}, \Delta\phi_{5-1}, \Delta\phi_{6-1}, \Delta\phi_{7-1}, \Delta\phi_{8-1}] = (-0.054\pi, -0.054\pi, 0, 0, -0.054\pi, -0.054\pi, 0)$ as a reference of the phase at the waveguide element 1 (see Fig.7). In the figure, the calculated field intensity and phase profiles, radiated from the PAA with 1 waveguide element and 8 elements, were also plotted. The calculated field profiles $E_{x,y}(x, y, z = 600)$ from the PAA were evaluated with a Kirchhoff integral as follows,

$$E_{x,y}(x, y, z) = \frac{ik}{2\pi z} \int_{-a/2}^{a/2} \int_{-a/2}^{a/2} dx' dy' \quad (1)$$

$$\times E_{x,y}(x', y') [\exp(-ikr)/r],$$

$$r = \sqrt{(x-x')^2 + (y-y')^2 + z^2},$$

where the coordinates of (x', y') and (x, y) were at the antenna aperture position ($z=0$) and at the radiated z position, and a was a side of the square-

waveguide, respectively. The beam was diverged in the large propagating length of $z=600$ mm with 1 waveguide element, but was focused with good directionality with the phased-array of the 8 waveguide elements. The measured intensity and phase profiles were well explained with the Kirchhoff integral calculation in general, but the measured intensity profile $E_y(y)$ was narrower than the calculated profile. The field $E_y(x', y')$ at the waveguide aperture was excited nearby at the waveguide boundary walls between 4 upper waveguides and lower ones. There were the direct couplings between the upper and lower waveguide series. The $E_y(y)$ radiated from each waveguide element was anti-symmetric in the y direction due to the direct coupling effect. Since there were only the 2 waveguide series in the developed PAA, the phased-array effect was weak to focus the beam in the y direction. The broader $E_x(y)$ and $E_y(y)$ profiles were obtained, compared with $E_x(x)$ and $E_y(x)$, due to the weak phased-array effect in the y direction.

The beam radiated from the PAA was focused well, in particular in the x direction. The PAA should be effective to take the large reflected wave signal in the reflectometry. Figure 9 illustrates the setup of the launching phased-array antenna and a receiving antenna for the reflectometry. Since the broader beam was obtained in the y direction, the significant reflected wave can be detected by the receiving antenna. In order to reduce the direct coupling effect between the launching and receiving antennae, the receiving antenna was set up at a distance from the launching PAA. Figure 10 shows the phase evolutions along the propagation in the SSB heterodyne detection, with and without removals of the Lissajou offsets (direct coupling effect), and with 1 or 8 waveguide elements at the PAA. Although the Lissajous offsets were numerically removed in the Fig.3, the offsets depended on the scanning operation-frequencies to obtain the density profile. In the Fig.9, the RF circuit components were added to remove the offsets. The offsets can be removed by the voltage control of the phase shifter and the attenuator with enough time resolution. The good phase evolution was obtained along the propagation even with 1 waveguide element by the additional RF circuits. The proper phase evolution was also obtained along the propagation using the PAA without the offset removal. Although the reflected wave signal was reduced in the QUEST experiments, the PAA will work well to obtain the significant reflected wave in the larger propagating length. The launching PAA and the additional RF circuits for the offset removal at the receiving antenna will be adopted in the reflectometry.

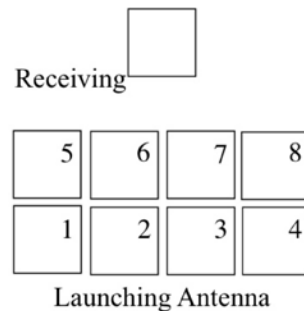


Fig. 9 : Illustration of launching phased-array and receiving antennae for the reflectometry in the low power test facilities.

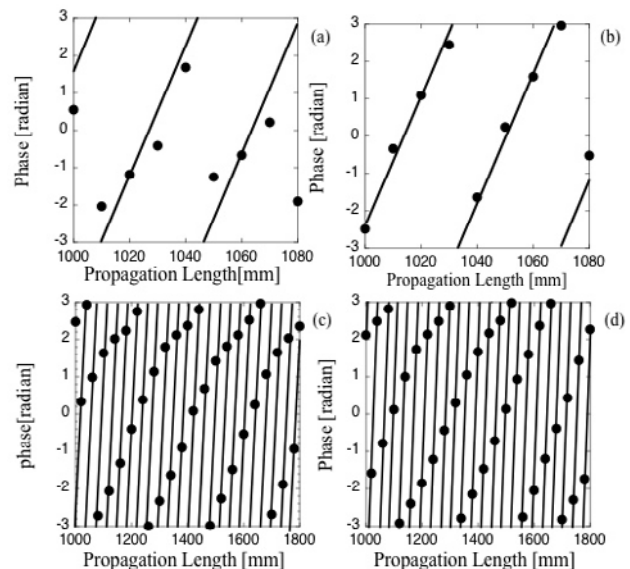


Fig. 10: Phase evolutions along the propagation: (a) without the offset removal by 1 waveguide element of the PAA, (b) with the offset removal by 1 waveguide element of the PAA, (c) without the offset removal by 8 waveguide elements of the PAA, and (d) with the offset removal by 8 waveguide elements of the PAA.

3.2 EBW Radiometry Use

The ray tracing and Fokker-Planck analyses were reported in the O-X-B scenario for the EBWH/CD experiments in the QUEST [1]. The incident oblique ECW met the O-mode cut off layer and was converted to the X-mode first. This X-mode was converted into the EBW at the upper hybrid resonance layer. The power deposition and driven current profiles were obtained in the analyses. The electron density and temperature, and plasma current profiles were assumed in the analyses. The electron temperature profile was also important, in particular to the driven current evaluation with the Fokker-Planck analysis, together with the density profile.

The EBW radiometry has been developed to measure time evolutions of electron temperature profiles in

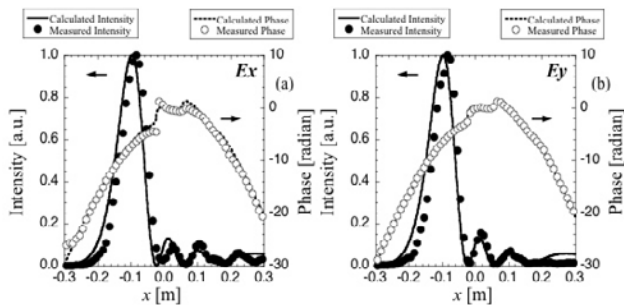


Fig. 11: Calculated and measured field intensity and phase profiles at $z=200$ mm, obliquely radiated from the PAA. (a): $E_x(x)$, (b): $E_y(x)$.

over-dense plasmas. The ECE radiometry was widely used to measure the electron temperature time evolutions, but the ECE cannot propagate outside the plasma due to the cut-off in the over-dense plasma. The ECW converted from the EBW as a reversal process of the mode conversion at the EBWH/CD propagated outside, and detected in the radiometry. The PAA was also considered as a receiving antenna in the radiometry to measure the oblique viewing EBW.

Figure 11 shows the field intensity and phase profiles $E_x(x)$ and $E_y(x)$ at $z=200$ mm, obliquely radiated from the PAA. Here, the phased-array was set as $[\Delta\phi_{2-1}, \Delta\phi_{3-1}, \Delta\phi_{4-1}, \Delta\phi_{5-1}, \Delta\phi_{6-1}, \Delta\phi_{7-1}, \Delta\phi_{8-1}] = (0.55\pi, 1.21\pi, 1.97\pi, 0, 0.55\pi, 1.21\pi, 1.97\pi)$ as a reference of the phase at the waveguide element 1. The measured fields were in excellent agreement with the calculated fields from the Kirchhoff integral. The oblique beam was obtained at two orthogonal electric field components by the phase adjustments between the PAA waveguide elements. The oblique viewing EBW emission will be observed by the precise phase-array measurements between the waveguide elements. The broadband OrthoMode Transducer (OMT) has been developed for the EBW radiometry to measure the two filed components. Figure 12 shows the frequency dependence of VSWR at the developed OMT. The low VSWR (< 2) was obtained in the broadband frequency range of 8-14.5 GHz, and it was expected to work well for the EBW radiometry. The ellipse polarization states for the X and O-modes can be measured by the intensity-ratio and phase-difference measurements between the two OMT ports at each PAA waveguide element.

4. Conclusion

The differential-phase reflectometry has been developed to measure the density profile evolution that is a key issue for the EBWH/CD experiments in the QUEST. The reflectometry based on the diode detection did not work correctly in the larger propagating length for the QUEST. The direct coupling compo-

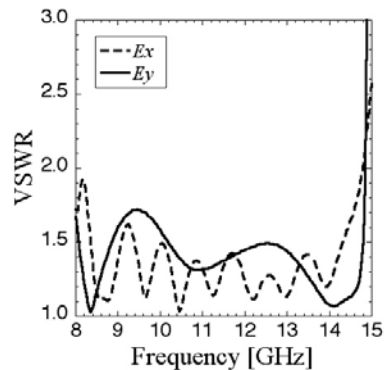


Fig. 12: Frequency dependence of VSWR at the developed orthomode transducer.

nent between the launching and receiving antennae affected the measured phase evolution along the propagation. The SSB heterodyne differential-phase reflectometry was proposed to remove the direct coupling component. The proper phase evolution in the larger propagation length was confirmed in the developed reflectometry at the low power test facilities. The phase time evolutions in the QUEST were also successfully measured, but the weak reflected-wave affected the measurements. In order to receive the larger reflected-wave, a phased-array antenna was proposed for the reflectometry. The oblique viewing EBW emission can be measured by the precise phase-array measurements between the PAA waveguide elements. The prototype phased-array antenna was designed using Kirchhoff integral calculation. The PAA was effective to excite straight and oblique beams for reflectometry and EBW radiometry. The broadband OMT has been developed to measure the O/X-mode polarizations in the radiometry. The developing phased-array antenna will be co-operated to measure the EBW emission to investigate the mode conversion phenomena, together with the reflectometry measurements.

5. Acknowledgment

This research was supported by the Ministry of Education, Science, Sports and Culture, Grant-in-Aid for Scientific Research (B), the NIFS LHD collaboration(NIFS09KOAHO24), and the NIFS bi-directional collaboration (NIFS09KUTR046).

- [1] H. Idei *et al.*, Journal of Plasma and Fusion Research Serie vol.8, 1104-1107 (2009).
- [2] H. Idei *et al.*, Proc. of 32nd Int. Conf. on Infrared and mm-Waves, 518 (2007).
- [3] H. Laqua *et al.*, Phy. Rev. Lett., **81** 2060 (1998).
- [4] S.J. Diem *et al.*, Phy. Rev. Lett., **103** 015002 (2009).